Article

*Discovery Medicine* 2026; 38(211): 2480–2495
https://doi.org/10.24976/Discov.Med.202638211.196

# NRBF2 Regulates Mitophagy via Interaction With AMBRA1 to Influence Sepsis-Induced Acute Lung Injury

Shuang Lu[1], Wenjing Zhao[1], Yujie Wang[1], Can Li[2], Jingzhang Zeng[1,*]

[1]Department of Infectious Diseases, The Second People's Hospital of Guiyang (Jinyang Hospital), 550081 Guiyang, Guizhou, China
[2]Department of Infectious Diseases, The Affiliated Hospital of Guizhou Medical University, 550001 Guiyang, Guizhou, China
*Correspondence: magiczjz@126.com (Jingzhang Zeng)
Submitted: 18 December 2025 Revised: 15 April 2026 Accepted: 24 April 2026 Published: 24 August 2026

**Background: Sepsis-induced acute lung injury (ALI) is a critical clinical challenge with substantial mortality. While mitophagy plays a pivotal role in ALI pathogenesis, the mechanisms underlying the involvement of nuclear receptor binding factor 2 (NRBF2), a key regulator of autophagy, in this process remain unexplored. Therefore, this study investigated whether NRBF2 regulates mitophagy by interacting with autophagy and beclin 1 regulator 1 (AMBRA1), thus influencing the progression of sepsis-induced ALI.**

**Methods: The cecal ligation and puncture mouse sepsis model and lipopolysaccharide (LPS)-induced endothelial cell model of ALI were used. NRBF2 expression was inhibited using lentiviral interference, and molecular biology and bioinformatics analyses were performed to investigate the effect of NRBF2 on mitophagy and ALI. The STRING database was used to predict the NRBF2–AMBRA1 interaction, which was subsequently validated using NRBF2 mutants with specific domain deletions.**

**Results: NRBF2 expression was significantly upregulated in septic ALI models ($p < 0.001$). *In vitro*, NRBF2 knockdown suppressed excessive LPS-induced mitophagy activation, improved mitochondrial function, and reduced the release of inflammatory factors ($p < 0.05$). In addition, the autophagy inhibitor chloroquine and mitochondrial division inhibitor 1 reversed mitochondrial dysfunction caused by NRBF2 overexpression ($p < 0.01$). *In vivo* experiments further confirmed that NRBF2 knockdown alleviated the pathological progression of sepsis-induced ALI ($p < 0.05$). Mechanistically, NRBF2 regulated mitophagy by interacting with AMBRA1 via its microtubule-interacting and trafficking domain ($p < 0.05$).**

**Conclusion: Our findings establish that NRBF2 exacerbates sepsis-induced ALI by promoting AMBRA1-dependent mitophagy, highlighting NRBF2 as a potential therapeutic target.**

**Keywords:** NRBF2; AMBRA1; mitophagy; acute lung injury; sepsis

## Introduction

Sepsis is a life-threatening syndrome characterized by organ dysfunction resulting from dysregulated host responses to infection [1]. The high incidence and mortality rates of sepsis have become a major global public health challenge [2]. Statistics show that millions of people worldwide are affected by sepsis annually, with a mortality rate as high as 22.5% [3]. The systemic inflammatory response in sepsis can lead to multiorgan failure, with the lungs being among the earliest and most susceptible organs. This response often manifests as acute lung injury (ALI), characterized by diffuse alveolar damage, refractory hypoxemia, and acute onset of respiratory distress [4]. Studies have shown that 25% to 50% of patients with sepsis experience ALI, with a mortality rate of 40% [5]. Currently, effective treatment options specifically targeting sepsis-induced ALI remain limited [6]. Therefore, a thorough understanding of the pathogenesis of sepsis-induced ALI and the identification of effective treatment strategies are critical.

Mitochondrial dysfunction, which impairs their function as cellular energy hubs and metabolic regulators, is a key contributor to sepsis-induced ALI [7]. Mitophagy is a selective form of autophagy that plays a crucial role in maintaining mitochondrial homeostasis and cellular survival by clearing damaged or dysfunctional mitochondria [8]. However, excessive mitophagy may worsen mitochondrial dysfunction and exacerbate inflammatory responses and cell apoptosis, thereby promoting the progression of ALI. A previous study has documented abnormal expression of mitophagy-related proteins, such as LC3-II and TOMM20, in a cecal ligation and puncture (CLP)–induced sepsis model [9]. This finding suggests that mitophagy dysfunction is an important mechanism underlying sepsis-induced ALI. However, the key regulatory molecules involved in this process and their mechanisms of action remain unclear.

Nuclear receptor binding factor 2 (NRBF2) is a 34 kDa protein widely distributed in the cytoplasm, nucleus, and autophagosomes. This protein participates in the initiation and progression of various diseases by positively regulating the autophagy initiation process [10]. A study has observed that NRBF2 can regulate malignant proliferation and drug resistance in tumor cells by activating the autophagy pathway [11]. Furthermore, increasing evidence suggests that the microtubule-interacting and trafficking (MIT) domain of NRBF2 plays a key role in autophagy regulation, influencing its initiation by interacting with proteins such as Atg14L [12]. Bioinformatic analysis of the Gene Expression Omnibus (GEO) database revealed significantly elevated NRBF2 expression in sepsis-induced ALI, suggesting its potential importance in this condition. Nonetheless, whether NRBF2, a positive regulator of autophagic initiation, modulates mitophagy during sepsis-induced ALI remains unknown.

Autophagy and beclin regulator 1 (AMBRA1) is a highly conserved scaffolding protein in vertebrates. This protein contains a WD40 domain and participates in the autophagy signaling network [13]. AMBRA1 regulates the activation of mitophagy by interacting with key proteins such as PTEN-induced kinase 1 (PINK1) and parkin [14]. STRING database predictions further suggest a potential interaction between NRBF2 and AMBRA1, implying a collaborative role in mitophagy regulation. Therefore, this study hypothesized that NRBF2 may bind to AMBRA1 via its MIT domain to coregulate excessive mitophagy, thereby exacerbating the progression of sepsis-related ALI.

Based on the above background, this study aimed to investigate whether NRBF2 regulates mitophagy by interacting with AMBRA1, thereby affecting sepsis-induced ALI. The intention was to provide a new theoretical foundation and identify potential therapeutic targets for this condition.

## Materials and Methods

### *Animal Models and Grouping*

A total of 54 C57BL/6J male mice aged 8–10 weeks (body weight: 20–25 g) were purchased from Beijing SPF Biotechnology Co., Ltd. The mice were housed in a specific pathogen free animal laboratory under controlled environmental conditions (12-h light–dark cycle, 21 °C–26 °C, 30%–70% humidity) for 1 week. All animal experiments were conducted according to the guidelines of the Ethics Committee of Guizhou Medical University (2503016) and adhered to the ethical standards for animal experimentation.

The sample size was determined using a priori power analysis of pilot serum and tumor necrosis factor-alpha (TNF-$\alpha$) data (Cohen's d = 1.45, G Power 3.1, *t*-test, $\alpha$ = 0.05 two-tailed, power = 0.8). Considering the exploratory nature of this study, the inherent biological variability in the CLP sepsis model, and the need for sufficient independent tissue samples for endpoint assays (e.g., lung wet/dry weight ratio), the final sample size was conservatively set to n = 9 per group. Post-hoc analysis confirmed an achieved power of 0.96, indicating that the study was adequately powered.

The mice were numbered and randomly assigned to groups using the Excel RAND function and then sorted in ascending order to ensure unbiased allocation. The animals were randomly assigned to two groups: Sham and Model, each consisting of n = 9 mice. Sepsis was induced using CLP. The mice were fasted for 12 h before surgery but had free access to water. Anesthesia was induced by intraperitoneal injection of tribromoethanol (T709120, Macklin, Shanghai, China) at a dose of 0.2 mL/20 g body weight (equivalent to 400 mg/kg). First, 50% of the cecum was ligated, followed by double puncture using an 18-gauge needle. The Sham surgery group underwent only the cecal exposure. Postoperatively, warm saline was administered intraperitoneally for fluid resuscitation. The mice were monitored twice daily. Of note, no analgesics or antibiotics were administered in this study. The depth of anesthesia was confirmed before surgery to ensure that the mice were completely unresponsive to pain stimuli; therefore, no additional analgesics were required during or after the procedure. Antibiotics were withheld as the CLP model relies on polymicrobial infection to induce systemic inflammation and sepsis. The use of antibiotics would interfere with the natural progression of infection and inflammatory responses.

For the NRBF2 knockdown experiment, lentiviral particles carrying NRBF2 short hairpin RNA (shRNA) or scrambled shRNA control were used. These particles were produced using the commercial lentiviral vector pLVX–shRNA2–copGFP-Puro (HG-VMH0884, Onuo, Changsha, China). The particles were injected into the model group mice via the tail vein 4 weeks before the surgery. The mice were randomly assigned to four groups: Sham, Model, Model+sh-NC, and Model+sh-NRBF2, with n = 9 mice per group. The surgical procedure was the same as that for the Model group. The mouse shRNA sequences are provided in **Supplementary File 1**.

All mice were euthanized via inhalation of an overdose of carbon dioxide ($CO_2$) in a standard euthanasia chamber. Death was confirmed based on respiratory arrest and lack of pedal reflex. Lung tissues were immediately collected, weighed, and fixed in 4% paraformaldehyde for subsequent analysis.

### *Cell Culture and Treatment*

Primary human pulmonary microvascular endothelial cells (HPMECs) were purchased from Shanghai Saibaikang Biotechnology Co., Ltd. (HUM-iCell-a001, China). HPMECs were identified by immunofluorescence. The normal human bronchial epithelial cell line BEAS-2B was obtained from Shanghai Enzyme Research Biotechnology Co., Ltd.

(CC-Y1066, China). BEAS-2B cells were authenticated by short tandem repeat (STR) analysis. Both cell lines tested negative for mycoplasma contamination. HPMECs were cultured in a specialized culture medium (iCell Bioscience, Shanghai, China), whereas BEAS-2B cells were maintained in Dulbecco's Modified Eagle Medium supplemented with 10% fetal bovine serum (10099141C, Gibco, Grand Island, NY, USA) and 1% penicillin–streptomycin (P1400, Solarbio, Beijing, China). All cells were cultured at 37 °C in a humidified incubator with 5% $CO_2$. To establish a sepsis-induced ALI cell model, the cells were treated with 1 µg/mL lipopolysaccharide (LPS; S1732-5mg, Beyotime, Shanghai, China) for 24 h.

In the interference experiment, NRBF2-specific shRNA (sh-NRBF2) or the nontargeting control shRNA (sh-NC) was cloned into the pLVX–shRNA2–copGFP–Puro lentiviral vector (HG-VMH0884, Onuo). The cells were transfected at 60%–70% confluence in six-well plates. The transfection complex was prepared by mixing 2.5 µg of plasmid DNA with 4 µL of Lipofectamine 8000 transfection reagent (C0533, Beyotime) in a total volume of 125 µL of serum-free medium according to the manufacturer's protocol. The mixture was incubated at room temperature for 15–20 min and then added evenly to each well. The empty vector was transfected in parallel. After culturing for 24–48 h, the cells were used for subsequent experiments. The cells were categorized into the following groups: Con, LPS, LPS+sh-NC, and LPS+sh-NRBF2.

In certain validation experiments, the NRBF2 gene was overexpressed using the plasmid pCDNA3.1-EGFP carrying the NRBF2 coding sequence (BR233, Feng Hui Bio., Changsha, China), with 2.5 µg transfected per well. The corresponding empty vector served as the overexpression negative control (OE-NC). Following transfection, the cells were pretreated with 100 µM chloroquine (CQ; IC4440, Solarbio) for 30 min or 10 µM Mdivi-1 (M0199, Sigma, St. Louis, MO, USA) for 2 h at 37 °C before stimulation with 1 µg/mL LPS for 24 h. The control group received an equivalent volume of the vehicle dimethyl sulfoxide (DMSO; 60313ES60, Yeasen, Shanghai, China). The cells were categorized into the following groups: Con, LPS, LPS+OE-NC, LPS+NRBF2-OE, LPS+CQ, and LPS+NRBF2-OE+CQ. The sequences for human NRBF2 shRNA and the NRBF2 overexpression construct are provided in **Supplementary File 1**.

### *Construction and Transfection of NRBF2 Domain-Deletion Mutants*

The wild-type human NRBF2 (MYC–WT–NRBF2) and its two domain-deletion mutants—lacking both the MIT (MYC–delMIT–NRBF2) and coiled-coil (MYC-delCCD–NRBF2) domains—were custom-designed and synthesized by Genecopoeia Inc. (Rockville, MD, USA) based on the pcDNA3.1-MYC vector backbone. The amino acid sequences of the deleted regions for both the MIT and CCD domains are listed in **Supplementary File 1**. For transient transfection, HPMECs were transfected with 2.5 µg of each plasmid using Lipofectamine 2000 (12566014, Thermo Fisher Scientific, Waltham, MA, USA) following the manufacturer's protocol. The cells were harvested 48 h post-transfection for analysis.

### *Hematoxylin and Eosin (H&E) Staining*

The lung tissue was fixed with 4% paraformaldehyde, embedded in paraffin, and sectioned at 4 µm. The lung sections were dewaxed and rehydrated, then stained with hematoxylin (G1004, Servicebio, Wuhan, China) for 5 min and eosin (G1001, Servicebio) for 2 min. After dehydration, clearing, and mounting with a mounting medium, the sections were examined under a microscope (DM500, Leica, Wetzlar, Hesse, Germany) to determine the extent of lung damage.

### *TermInal Deoxynucleotidyl Transferase dUTP Nick End Labeling (TUNEL) Staining*

Mouse lung tissues were fixed in 4% paraformaldehyde, embedded in paraffin, and sectioned into 4 µm-thick slices. After deparaffinization and rehydration, the sections were processed according to the instructions of the TUNEL detection kit (G1501, Servicebio). First, the tissue sections were treated with 20 µg/mL proteinase K at 37 °C for 20 min to expose DNA nicks. Subsequently, 50 µL of TUNEL reaction solution (containing terminal deoxynucleotidyl transferase enzyme and fluorescein isothiocyanate deoxyuridine triphosphate) was applied to each section, and the sections were incubated at 37 °C in the dark for 1 h. Subsequently, the sections were washed four times with phosphate-buffered saline (PBS), and the nuclei were stained with 4′,6-diamidino-2-phenylindole (DAPI, C1006, Beyotime) at room temperature for 8 min. Finally, the sections were mounted with an anti-fade mounting medium. The slides were observed under a fluorescence microscope (BZ-X800, Keyence, Osaka, Japan), with fluorescein isothiocyanate (FITC) green fluorescence indicating apoptotic cells and DAPI blue fluorescence labeling all nuclei. Three nonoverlapping fields were randomly selected for each section, and the percentage of TUNEL-positive cells was calculated using the ImageJ software (Version 1.48, National Institutes of Health, Bethesda, MD, USA) as follows: TUNEL-positive cells (%) = (number of TUNEL-positive cells / total number of DAPI-positive cells) × 100%.

### *Lactate Dehydrogenase (LDH) Activity*

After anesthetizing the mice, a plastic cannula was inserted into the trachea and secured with a 4-0 suture. One milliliter of sterile saline was slowly injected, and the lungs were gently compressed three times to obtain the bronchoalveolar lavage fluid (BALF). The BALF sample was centrifuged at 4 °C for 10 min, and the supernatant was

**Table 1. qRT-PCR primers.**

| Gene | Forward sequence (5′-3′) | Reverse sequence (5′-3′) |
|---|---|---|
| *NRBF2* (Mouse) | AGACTCCTGAAAGGCACAGC | ATGTCCTCCGAGAGCTCCAT |
| *NRBF2* (Human) | AGGACCCCTCAACCTGCATA | ATACATGGCTCTGCTGGCTC |
| *β-actin* (Human/Mouse) | CTACTCCACTGTGGCTCTGGTG | TTGTGGATGGCAGAAGCCTTGG |

qRT-PCR, Quantitative real-time polymerase chain reaction; *NRBF2,* nuclear receptor binding factor 2.

collected and stored at –80 °C. The total protein concentration was subsequently measured using the bicinchoninic acid (BCA) method, and LDH activity was detected according to the instructions of the LDH assay kit (E-BC-K046-M, Elabscience, Wuhan, China).

### *Lung Wet/Dry Weight Ratio Measurement*

Lung tissue was collected from the right upper lobe of each group of mice; the surface liquid was blotted dry with filter paper, and the tissue was placed in a dry, peeled Eppendorf tube. The wet weight was immediately measured and recorded using an analytical balance. The samples were then placed in a 60 °C vacuum oven for 72 h of drying, with weights recorded every 24 h until two consecutive weighings showed no change, indicating a constant weight (lung dry weight). Finally, the degree of pulmonary edema was assessed by calculating the wet-to-dry weight ratio of the lung tissue.

### *Enzyme-Linked Immunosorbent Assay (ELISA)*

Mouse TNF-$\alpha$ (E-EL-M3063), mouse interleukin (IL)-1$\beta$ (E-EL-M0037), and mouse IL-6 (E-EL-M0044) ELISA kits (Elabscience) were used to determine the levels of TNF-$\alpha$, IL-1$\beta$, and IL-6 in the serum. Supernatant samples were collected and tested according to the kit instructions. Absorbance (optical density, OD) values were measured using a microplate reader (Multiskan FC, Thermo Fisher Scientific, Waltham, MA, USA).

### *Quantitative Real-Time Polymerase Chain Reaction (qRT-PCR)*

qRT-PCR was used to assess NRBF2 expression levels in HPMECs and lung tissues. First, RNA was extracted using TRIzol reagent (G3013, Servicebio) and then reverse-transcribed into cDNA using the PrimeScript™ RT kit (RR037Q, Takara, Japan). qRT-PCR experiments were performed using TB Green® Premix Ex Taq™ II (RR820Q, Takara), with $\beta$-actin as the internal control. The relative expression levels of the target genes were analyzed using the $2^{-\Delta\Delta Ct}$ method, with each sample tested in triplicate. The primers used in qRT-PCR are furnished in Table 1.

### *Western Blotting (WB)*

Total protein was extracted from cells and tissues using the radioimmunoprecipitation assay (RIPA) buffer (BL504A, Biosharp, Hefei, China). Protein concentration was determined using the BCA protein assay kit (Biosharp). Subsequently, 10% sodium dodecyl sulfate polyacrylamide gel electrophoresis was performed to separate the protein samples. The separated proteins were transferred to a polyvinylidene fluoride membrane. The membrane was incubated overnight at 4 °C with the following primary antibodies: anti-NRBF2 (1:1000 dilution, TP73269, Abmart, Shanghai, China), anti-TOM20 (1:1000 dilution, ab186735, Abcam, UK), anti-PINK1 (1:1000 dilution, 23274-1-AP, Proteintech), anti-parkin (1:1000 dilution, ab77924, Abcam), anti-p62 (1:1000 dilution, ab109012, Abcam), anti-LC3 (1:1000 dilution, L8918, Sigma), and anti-$\beta$-actin (1:1000 dilution, ab8226, Abcam). Then, horseradish peroxidase–conjugated immunoglobulin G (1:5000 dilution, ab6721/ab6789, Abcam) was incubated at 37 °C for 1 h for staining. Finally, the immunoreactive bands were analyzed using ImageJ (Version 1.48, National Institutes of Health).

### *Cell Counting Kit-8 (CCK-8)*

Cells in the logarithmic growth phase were collected, digested, and their concentration adjusted to $1 \times 10^6$/mL. The cell suspension was seeded into a 96-well plate with three replicates per group and incubated at 37 °C and 5% $CO_2$. After 24 h, 10 µL of CCK-8 reagent (40203ES60, Yeasen, China) was added to each well, and the cells were cultured for an additional 1 h. The absorbance (OD value) at 450 nm was measured using a microplate reader (Multiskan FC, Thermo Fisher Scientific) to assess cell viability.

### *Flow Cytometry*

Log-phase cells were digested with 0.25% trypsin, centrifuged at 1000 rpm, and resuspended in 1× binding buffer to adjust the cell concentration to 1–5 $\times$ $10^6$ cells/mL.

Apoptosis was assessed using the Annexin V-FITC Apoptosis Detection Kit (G1511, Servicebio). Then, 100 µL of the cell suspension was collected, and 5 µL of Annexin V-FITC and 5 µL of PI were added. The mixture was incubated at room temperature for 10 min.

Mitochondrial reactive oxygen species (mtROS) levels were determined using the MitoSOX™ Red mitochondrial superoxide indicator (M36009, Thermo Fisher Scientific). According to the manufacturer's instructions, an appropriate amount of MitoSOX™ reagent was added to the cells, mixed well, and incubated at room temperature for 30 min.

Finally, the cells were analyzed using a flow cytometer (NovoCyte, Agilent, USA).

### *Immunofluorescence (IF)*

The cell samples were washed with PBS and fixed with 4% paraformaldehyde. Subsequently, the samples were placed in a 48-well plate, then permeabilized with 1% Triton X-100 and blocked with 200 µL of blocking solution. For CD31 single staining, the cells were incubated overnight at 4 °C with anti-CD31 (1:100 dilution, 11265-1-AP, Proteintech, Wuhan, China), washed with PBS, and then incubated with CoraLite488-conjugated goat anti-rabbit IgG (1:500 dilution, SA00013-2, Proteintech) at room temperature in the dark for 1 h. For double staining, the cells were incubated overnight at 4 °C with a mixture of primary antibodies: anti-LC3B (1:100 dilution, K009582P, Solarbio) and anti-COXIV (1:100 dilution, 66110-1-Ig, Proteintech, Wuhan, China) or anti-NRBF2 (1:100 dilution, M09144-1, Boster, Wuhan, China) and anti-AMBRA1 (1:100 dilution, 13762-1-AP, Proteintech). After washing with PBS, the cells were incubated with diluted solutions of the corresponding secondary antibodies (FITC-goat anti-rabbit IgG H&L [1:100 dilution, A0562, Beyotime] or Cy3-labeled goat anti-mouse IgG [1:100 dilution, A0521, Beyotime]) and incubated at room temperature in the dark for 1 h. The nuclei were stained with DAPI (C1006, Beyotime), washed with PBS, and mounted. Finally, images were acquired and analyzed under a fluorescence microscope (BZ-X800, Keyence). For quantitative analysis of LC3B, the number of LC3B puncta per cell was counted using ImageJ (Version 1.48, National Institutes of Health), and the quantification was based on LC3B puncta/cells. For quantitative analysis of NRBF2, AMBRA1, and COXIV, the mean fluorescence intensity was measured using ImageJ (Version 1.48, National Institutes of Health).

For lung tissues, fresh samples were stored at –80 °C, embedded in optimal cutting temperature compound (G6059, Servicebio), and sectioned at 8 µm. The sections were permeabilized with 0.2% Triton X-100 (P0096, Beyotime) for 15 min and blocked with 3% bovine serum albumin (A8010, Solarbio) for 30 min. The nuclei were stained with DAPI (G1012, Servicebio) for 15 min. After mounting, the sections were observed under a fluorescence microscope (BZ-X800, Keyence). Green fluorescent protein fluorescence was used to trace lentiviral infection.

### *Mito-Tracker Staining*

Mito-Tracker Red CMXRos (C1035, Beyotime) was used to observe mitophagy. The Mito-Tracker stock solution was prepared in anhydrous DMSO according to the instructions and then diluted with preheated cell culture medium to obtain working solutions of 20–200 nM. When the cell density reached 80%–90%, the original medium in the culture dish was removed and the staining working solution was added. The cells were incubated at 37 °C with 5% $CO_2$, protected from light, for 15–30 min. After staining, the staining solution was removed and the cells were washed with PBS. Finally, the cells were observed and photographed under a fluorescence microscope (BZ-X800, Keyence).

### *Detection of ATP*

An appropriate volume of lysis buffer was added to the cells. The cells were lysed on ice, then centrifuged at 12,000 rpm at 4 °C for 5 min to collect the supernatant. The standard curve was prepared according to the instructions of the Enhanced ATP Assay Kit (S0027, Beyotime). Subsequently, an appropriate volume of ATP detection reagent was diluted with the diluent at a 1:4 ratio to prepare the ATP detection working solution. Finally, 100 µL of the ATP detection working solution was added to the detection well or tube, and the relative light units value was measured using a chemiluminescence detector (Multiskan FC, Thermo Fisher Scientific).

### *JC-1 Staining*

Mitochondrial membrane potential was measured using JC-1 staining according to the instructions of the JC-1 assay kit (C2006, Beyotime). When the cell density reached 80%–90%, the culture medium was removed and the JC-1 staining working solution was added. The cells were subsequently placed in a cell culture incubator for 20 min. After incubation, the supernatant was removed and the cells were washed twice with 1× JC-1 staining buffer. The stained cells were observed under a fluorescence microscope (IX73, Olympus, Tokyo, Japan) and photographed for record-keeping. For flow cytometry analysis, the stained cells were harvested, resuspended in 1× JC-1 staining buffer, and analyzed using a flow cytometer (NovoCyte, Agilent). The percentage of cells with depolarized mitochondrial membrane potential was determined by determining the ratio of JC-1 monomers (green fluorescence) to aggregates (red fluorescence).

### *Co-Immunoprecipitation (Co-IP)*

The protein–protein interaction between NRBF2 and AMBRA1 was validated using a Co-IP kit (P2179S, Beyotime). The cells were lysed in RIPA lysis buffer on ice for 30 min, and the supernatant was collected after centrifugation. Protein concentrations were measured using the BCA method, and 500 µg of protein per sample was used for the experiment. A portion of the supernatant was set aside as the "input" control. The remaining supernatant was mixed with 1 µg of anti-NRBF2 antibody (TP73269, Abmart) or an equivalent amount of rabbit IgG (ab172730, Abcam) and Protein A/G magnetic beads, then incubated overnight at 4 °C. The next day, the beads were washed three times with prechilled RIPA buffer. Finally, 1× sodium dodecyl sulfate loading buffer was added, and the bound proteins were eluted by heating at 95 °C for 5 min. The eluted samples

were analyzed using WB with an anti-AMBRA1 antibody (1:1000, 13762-1-AP, Proteintech) to detect the coprecipitated proteins.

### *Bioinformatics Analysis*

Bioinformatics analysis was performed to investigate the expression characteristics and interaction relationships of NRBF2 in sepsis. First, the sepsis model dataset GSE269740 was downloaded from the GEO database, and the GEO2R online tool was used to analyze NRBF2 expression differences between the CLP and control groups. Subsequently, the STRING database (https://string-db.org/) was used to predict NRBF2-interacting proteins, revealing a potential interaction between NRBF2 and AMBRA1. All analyses were performed using R software (version 4.2.1, R Core Team, Vienna, Austria) and related bioinformatics packages.

### *Statistical Analysis*

All experimental data are presented as mean $\pm$ standard deviation. Statistical analysis was performed using GraphPad Prism 9.6 software (GraphPad Software, USA). For comparisons between two groups, a two-tailed unpaired Student's *t*-test was used. For comparisons among three or more groups, one-way analysis of variance was applied, followed by Tukey's test for post hoc multiple comparisons. $p < 0.05$ was considered significant.

## Results

### *NRBF2 Expression Was Elevated in Sepsis-Induced ALI*

Analysis of the GEO database revealed significant upregulation of NRBF2 expression in the CLP group (Fig. 1A). To understand the role of NRBF2 in sepsis-induced ALI, a mouse sepsis model was initially established using the CLP method. The timeline of the animal experiments is depicted in Fig. 1B. LDH activity in BALF was significantly elevated in the Model group (Fig. 1C, $p < 0.01$). H&E staining was performed to evaluate lung tissue damage. No significant pathological changes were observed in the Sham group. However, CLP induction caused severe lung damage in mice, characterized by alveolar collapse, interstitial edema, thickened alveolar walls, and massive inflammatory cell infiltration (Fig. 1D). Measurement of lung wet weight/dry weight confirmed worsening pulmonary edema in septic mice (Fig. 1E, $p < 0.01$). In addition, ELISA revealed that the levels of the inflammatory factors TNF-$\alpha$, IL-1$\beta$, and IL-6 were significantly elevated in the serum of CLP-induced mice (Fig. 1F, $p < 0.001$). Importantly, qRT-PCR and WB detection indicated that NRBF2 expression was significantly upregulated in the lung tissue of the Model group (Fig. 1G,H, $p < 0.001$).

To validate the above results *in vitro*, an ALI cell model was constructed using LPS-induced HPMECs. The purity of primary HPMECs was confirmed using CD31 IF staining (**Supplementary Fig. 1**). CCK-8 results showed that cell viability was significantly reduced in the LPS group, indicating that LPS successfully induced cell damage (Fig. 1I, $p < 0.001$). Moreover, flow cytometry analysis revealed a significant increase in apoptosis rates in the LPS group (Fig. 1J,K, $p < 0.001$). qRT-PCR and WB results further confirmed that NRBF2 expression was significantly upregulated in LPS-induced cells, consistent with the animal experiment results (Fig. 1L,M, $p < 0.001$). Collectively, these findings establish that NRBF2 expression was abnormally elevated in sepsis-induced ALI, suggesting its potential role in disease pathogenesis.

### *NRBF2 Knockdown Inhibited Mitophagy and Alleviated Mitochondrial Dysfunction*

LPS-induced HPMECs were transfected with sh-NC or sh-NRBF2. The efficiency of NRBF2 knockdown in HPMECs was validated using qRT-PCR and WB, which showed a significant reduction in NRBF2 expression with sh-NRBF2-1 and sh-NRBF2-2 (**Supplementary Fig. 2A,B**, $p < 0.01$). Therefore, sh-NRBF2-2, which exhibited higher knockdown efficiency, was selected for subsequent experiments. Next, in the LPS-induced ALI cell model, NRBF2 expression level was confirmed to be further reduced after NRBF2 interference (**Supplementary Fig. 2C,D**, $p < 0.05$). In functional assays, CCK-8 detection demonstrated that LPS-induced reduction in cell viability was partially restored by NRBF2 knockdown (Fig. 2A, $p < 0.01$). In addition, WB results revealed that LPS induction decreased mitophagy markers Tom20 and p62, increased PINK1 and parkin expression levels, and the LC3-II/LC3-I ratio. By contrast, sh-NRBF2 treatment reversed these changes, indicating that mitophagy was inhibited (Fig. 2B, **Supplementary Fig. 2E**, $p < 0.05$). IF and Mito-Tracker staining further confirmed that NRBF2 knockdown reduced LC3B colocalization with mitochondria and ameliorated mitochondrial morphological abnormalities (Fig. 2C,D, **Supplementary Fig. 2F,G**, $p < 0.001$). Mitochondria are organelles essential for energy metabolism, reactive oxygen species (ROS) production, and cell proliferation [15]. Experiments showed that LPS induction reduced the ATP synthesis rate (Fig. 2E), increased mtROS levels (Fig. 2F), disrupted mitochondrial membrane potential (Fig. 2G, **Supplementary Fig. 2H**), and increased the cell apoptosis rate (Fig. 2H), whereas sh-NRBF2 treatment reversed these trends ($p < 0.001$).

Parallel experiments conducted in human normal lung epithelial cells (BEAS-2B) yielded consistent findings. The knockdown efficiency of NRBF2 was successfully validated in BEAS-2B cells, with sh-NRBF2-1 exhibiting the highest efficiency among the two shRNA sequences tested; therefore, it was selected for subsequent experiments (**Supplementary Fig. 3A,B**, $p < 0.001$). NRBF2 knockdown reduced its own expression in BEAS-2B cells

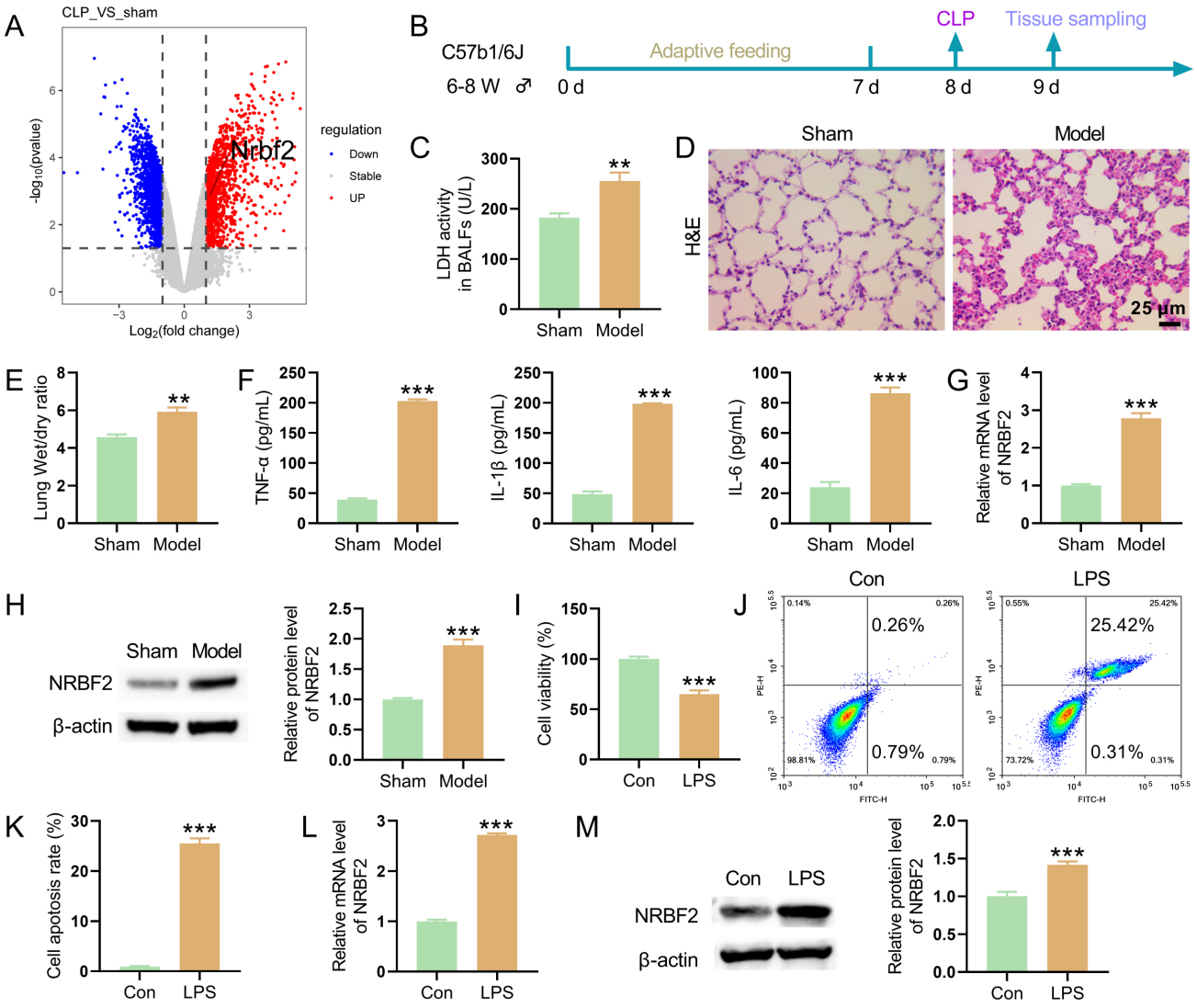


**Fig. 1. Validation of NRBF2 expression in sepsis-induced ALI.** The mouse sepsis model was constructed using CLP surgery. *In vivo* experimental groups: Sham, Model. (A) GEO database analysis of NRBF2 expression in the CLP model. (B) Animal experiment timeline. (C) The LDH assay kit was used to detect LDH activity in BALF. (D) Pathological changes in the mouse lung tissue were observed using H&E staining. (E) Measurement of lung wet weight/dry weight (W/D) ratio. (F) ELISA was used to measure the levels of TNF-$\alpha$, IL-1$\beta$, and IL-6 in the serum. (G,H) The expression level of NRBF2 in lung tissues was evaluated using qRT-PCR and WB. LPS-induced ALI cell model in sepsis was established using HPMECs. *In vitro* experimental groups: Con, LPS. (I) The CCK-8 assay was performed to assess cell viability. (J,K) The rate of cell apoptosis was evaluated using flow cytometry. (L,M) qRT-PCR and WB were performed to assess the expression level of NRBF2. n = 6 (C); n = 3 (D–M). $^{**}p < 0.01$, $^{***}p < 0.001$ vs. Sham or Con. NRBF2, nuclear receptor binding factor 2; ALI, acute lung injury; CLP, cecal ligation and puncture; GEO, Gene Expression Omnibus; LDH, Lactate dehydrogenase; BALF, bronchoalveolar lavage fluid; H&E, Hematoxylin and eosin; ELISA, Enzyme-linked immunosorbent assay; TNF-$\alpha$, tumor necrosis factor-alpha; IL, interleukin; qRT-PCR, Quantitative real-time polymerase chain reaction; WB, Western blotting; LPS, lipopolysaccharide; HPMECs, human pulmonary microvascular endothelial cells; CCK-8, Cell counting kit-8.

and reversed LPS-induced alterations in mitophagy markers (Tom20, p62, PINK1, parkin, and LC3-II/I) (Fig. 3A, **Supplementary Fig. 3C–E**, $p < 0.01$), reduced LC3B-mitochondria colocalization (Fig. 3B, **Supplementary Fig. 3F**, $p < 0.001$), attenuated the rise in mtROS levels (Fig. 3C, $p < 0.001$), mitigated mitochondrial membrane potential disruption (Fig. 3D, $p < 0.05$), and reduced the increase in apoptosis rate (Fig. 3E, $p < 0.001$). These results indicate that NRBF2 knockdown effectively inhibited LPS-induced excessive mitophagy and improved mitochondrial dysfunction in both pulmonary endothelial and epithelial cells.

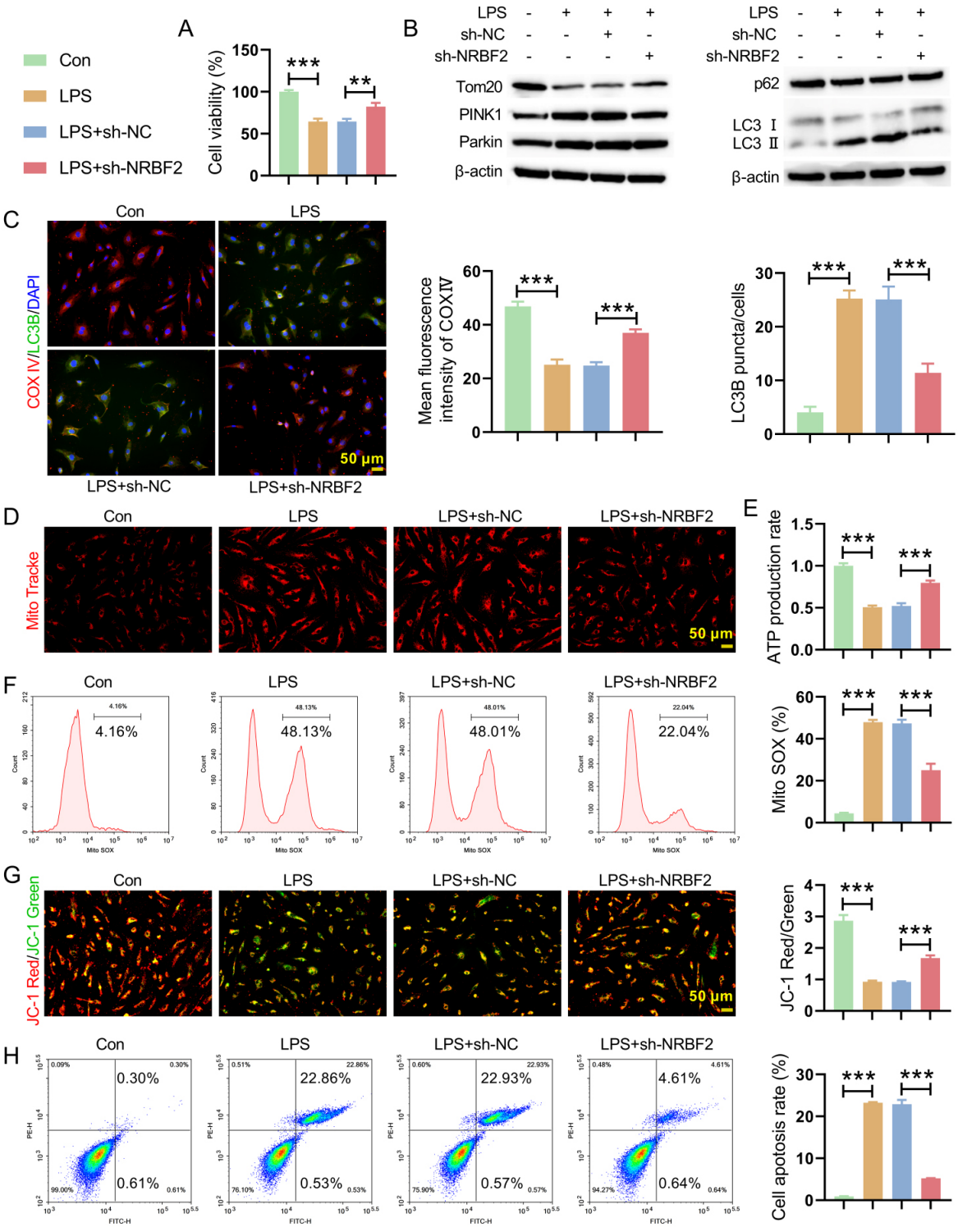


**Fig. 2. Effects of NRBF2 knockdown on mitophagy and mitochondrial function in HPMECs.** LPS-induced HPMECs were transfected with sh-NC or sh-NRBF2. Experimental groups: Con, LPS, LPS+sh-NC, and LPS+sh-NRBF2. (A) CCK-8 was employed to test cell viability. (B) WB was performed to assess the expression levels of Tom20, PINK1, parkin, p62, and LC3-II/LC3-I. (C) The colocalization of LC3B with mitochondria was observed using IF. (D) Mito-Tracker staining was used to determine mitochondrial morphology. (E) An enhanced ATP assay kit was applied to detect the ATP production rate. (F) mtROS was detected using flow cytometry. (G) JC-1 staining under fluorescence microscopy was performed to evaluate mitochondrial membrane potential. (H) The rate of cell apoptosis was measured using flow cytometry. n = 3. ** $p < 0.01$, *** $p < 0.001$ vs. Con or LPS+sh-NC. sh-NC, nontargeting control shRNA; PINK1, PTEN-induced kinase 1; LC3, Microtubule-associated protein 1 light chain 3; IF, Immunofluorescence; ATP, Adenosine triphosphate; mtROS, Mitochondrial reactive oxygen species; JC-1, Tetraethylbenzimidazolylcarbocyanine iodide.

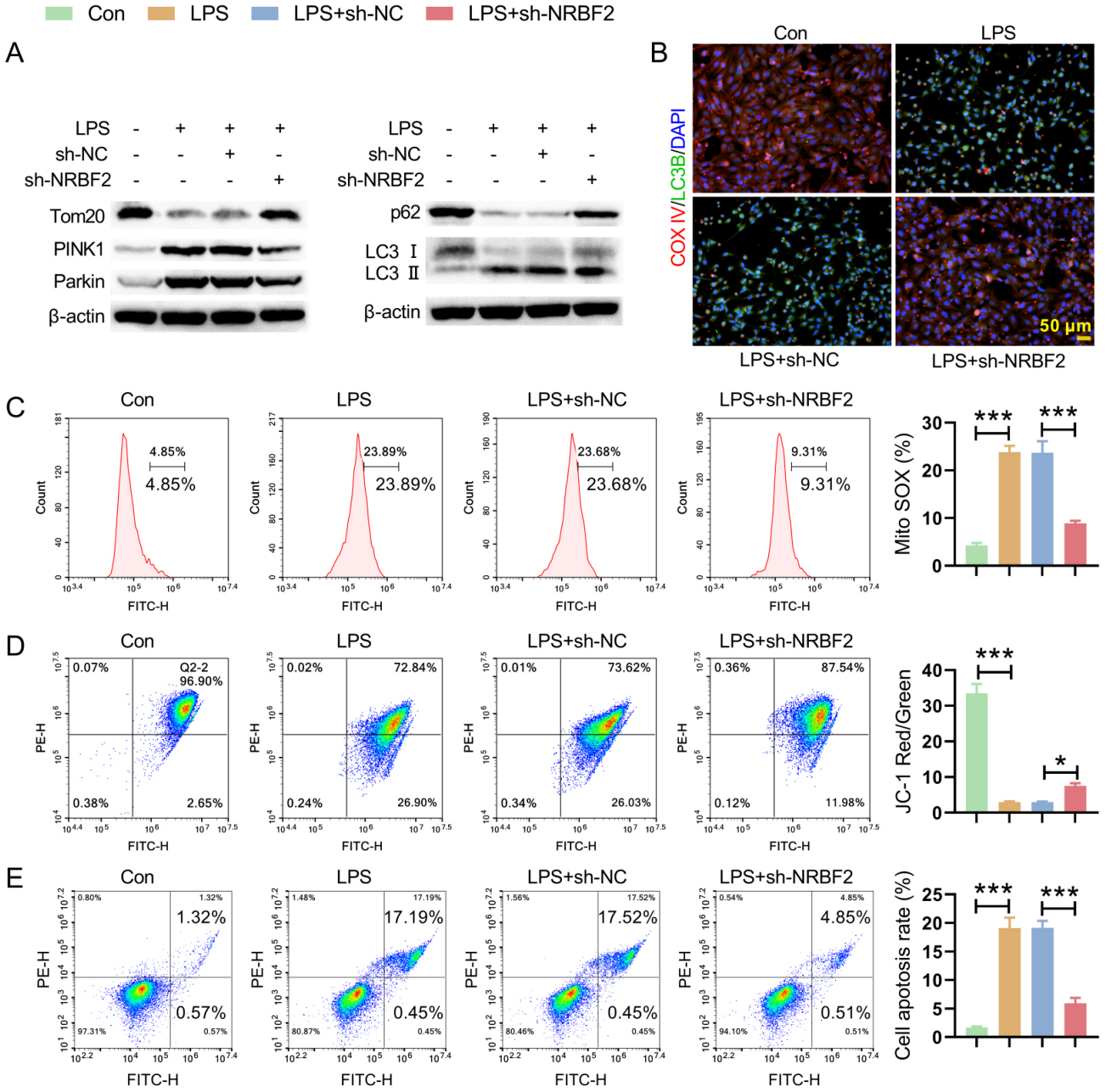


**Fig. 3. Effects of NRBF2 knockdown on mitophagy and mitochondrial function in BEAS-2B cells.** LPS-induced BEAS-2B cells were transfected with sh-NRBF2. Experimental groups: Con, LPS, LPS+sh-NC, and LPS+sh-NRBF2. (A) Protein levels of Tom20, PINK1, parkin, and p62 and the LC3-II/LC3-I ratio were assessed using WB. (B) Colocalization of LC3B with mitochondria was detected using IF. (C–E) Flow cytometry was performed to assess mtROS, mitochondrial membrane potential, and apoptosis. n = 3. * $p < 0.05$, *** $p < 0.001$ vs. Con or LPS+sh-NC. BEAS-2B, Bronchial Epithelium transformed with Ad12-SV40 2B.

### *Autophagy and Mitophagy Inhibitors Reversed Excessive Mitophagy and Mitochondrial Dysfunction Induced by NRBF2 Overexpression*

To further investigate the specific role of NRBF2-driven mitophagy, LPS-induced HPMECs were transfected with an NRBF2 overexpression plasmid and cotreated with either the general autophagy inhibitor CQ or the mitophagy inhibitor Mdivi-1. The overexpression efficiency of NRBF2 was successfully validated (**Supplementary Fig. 4A,B**). The results showed that CQ or Mdivi-1 treatment significantly reduced both mRNA and protein expression levels of NRBF2 (Fig. 4A,B, $p < 0.001$). The CCK-8 assay demonstrated that NRBF2 overexpression decreased cell viability, a reduction that could be reversed by cotreatment with CQ or Mdivi-1 (Fig. 4C, $p < 0.01$). WB analysis revealed that NRBF2 overexpression downregulated Tom20 and p62, upregulated PINK1 and parkin, and increased the LC3-II/LC3-I ratio. These changes were re-

versed by CQ or Mdivi-1 treatment (Fig. 4D, **Supplementary Fig. 4C**, $p < 0.001$). IF staining further confirmed that CQ or Mdivi-1 treatment significantly reduced the colocalization of LC3B with mitochondria (Fig. 4E, **Supplementary Fig. 4D**, $p < 0.01$). At the functional level, NRBF2 overexpression significantly increased mtROS production (Fig. 4F,G, $p < 0.001$), decreased ATP synthesis (Fig. 4H, $p < 0.001$), reduced mitochondrial membrane potential (Fig. 4I,J, $p < 0.001$), and increased cell apoptosis (Fig. 4K,L, $p < 0.001$). Combined treatment with CQ or Mdivi-1 effectively reversed the aforementioned alterations induced by NRBF2 overexpression ($p < 0.001$). Together, these results indicate that both CQ and Mdivi-1 consistently reversed the detrimental phenotypes induced by NRBF2 overexpression, asserting that the pathogenic effects of NRBF2 are specifically dependent on excessive mitophagy.

### *NRBF2 Regulated Mitophagy by Interacting With AMBRA1 via the MIT Domain*

To elucidate the molecular mechanism by which NRBF2 regulates mitophagy, plasmids with deletions in the MIT or CCD regions of NRBF2 were constructed and transfected into HPMECs. Prediction using the STRING database revealed a potential interaction between NRBF2 and AMBRA1 (Fig. 5A). IF and Co-IP experiments confirmed the colocalization and direct interaction between NRBF2 and AMBRA1 (Fig. 5B,C, **Supplementary Fig. 5A**, $p < 0.001$). WB results showed that, compared with the LPS+WT-NRBF2 group, MIT domain deletion increased the expression of mitophagy-related proteins Tom20 and p62, decreased the expression of PINK1 and parkin, and reduced the LC3-II/LC3-I ratio ($p < 0.05$). By contrast, deletion of the CCD region had no significant effect (Fig. 5D). In addition, IF analysis revealed that MIT deficiency led to decreased LC3B green fluorescence intensity and reduced large-area overlaps in the colocalization region (Fig. 5E, **Supplementary Fig. 5B**, $p < 0.01$). Flow cytometry showed that the deletion of the MIT region also reduced the apoptosis rate (Fig. 5F, $p < 0.001$). These results suggest that NRBF2 interacts with AMBRA1 via its MIT region, thereby regulating mitophagy.

### *Interfering With NRBF2 Expression Alleviated Sepsis-Induced ALI In Vivo*

Based on the results of prior cell-based experiments, this study further validated the alleviating effect of NRBF2 expression interference on sepsis-induced ALI at the animal level. Initially, the infection and knockdown efficiency of lentivirus-mediated NRBF2 were verified. Lentiviral particles containing NRBF2 interference plasmids (sh-NRBF2-1 and sh-NRBF2-2) or empty vector plasmid (sh-NC) were injected into model mice via the tail vein. Lung tissues were collected after CLP modeling for detection. The experimental timeline is illustrated in Fig. 6A. IF results showed that FITC-positive signals were observed in the lung tissues of mice in all groups, confirming successful lentiviral infection (**Supplementary Fig. 6A**). qRT-PCR and WB results showed that the mRNA and protein expression levels of NRBF2 in lung tissues were significantly reduced in both the sh-NRBF2-1 and sh-NRBF2-2 groups compared with the sh-NC group (**Supplementary Fig. 6B,C**, $p < 0.001$). Of these, the downregulation was more pronounced in the Model+sh-NRBF2-1 group; therefore, the sh-NRBF2-1 sequence was selected for subsequent experiments.

Based on this finding, the effect of NRBF2 knockdown on sepsis-induced ALI was further investigated. Compared with the Model+sh-NC group, the mice in the Model+sh-NRBF2 group exhibited reduced LDH activity in BALF and decreased lung wet/dry weight ratio (Fig. 6B,C, $p < 0.05$). H&E staining results indicated that compared with the Model+sh-NC group, NRBF2 knockdown ameliorated structural damage to the lung tissue, decreased inflammatory cell infiltration, and reduced bleeding levels caused by CLP surgery (Fig. 6D). ELISA indicated that sh-NRBF2 treatment significantly reduced the increase in TNF-$\alpha$, IL-1$\beta$, and IL-6 levels in the serum of CLP-induced mice (Fig. 6E, $p < 0.001$). In addition, qRT-PCR and WB confirmed that NRBF2 knockdown suppressed NRBF2 expression (Fig. 6F,G, $p < 0.05$). Furthermore, WB results showed that CLP induction significantly decreased the mitophagy markers Tom20 and p62 and increased PINK1 and parkin expression levels and the LC3-II/LC3-I ratio. However, this effect was significantly reversed when the mice were treated with sh-NRBF2 (Fig. 6H,I, $p < 0.001$). TUNEL assay revealed increased apoptosis rates in the Model group. Nonetheless, NRBF2 knockdown reversed this result (Fig. 6J, $p < 0.01$). In summary, these data suggest that interfering with NRBF2 expression alleviates sepsis-induced ALI by inhibiting autophagy.

## Discussion

Sepsis is a life-threatening systemic inflammatory syndrome caused by a dysregulated host response to infection. Sepsis has long been a focus of medical research, particularly owing to the high incidence and mortality of sepsis-induced ALI [16]. Despite significant progress in recent years in understanding sepsis and its complications, the specific mechanisms underlying ALI and effective treatment strategies remain unclear. Hence, this study focused on the role of NRBF2 in sepsis-induced ALI, revealing, via *in vitro* and *in vivo* experiments, its key role in regulating mitophagy and thereby alleviating disease progression. This research provides new insights into the pathogenesis of sepsis-induced ALI and offers a foundation for developing novel therapeutic strategies.

NRBF2, a positive regulator of autophagy initiation, has been reported to play a significant role in tumorigenesis

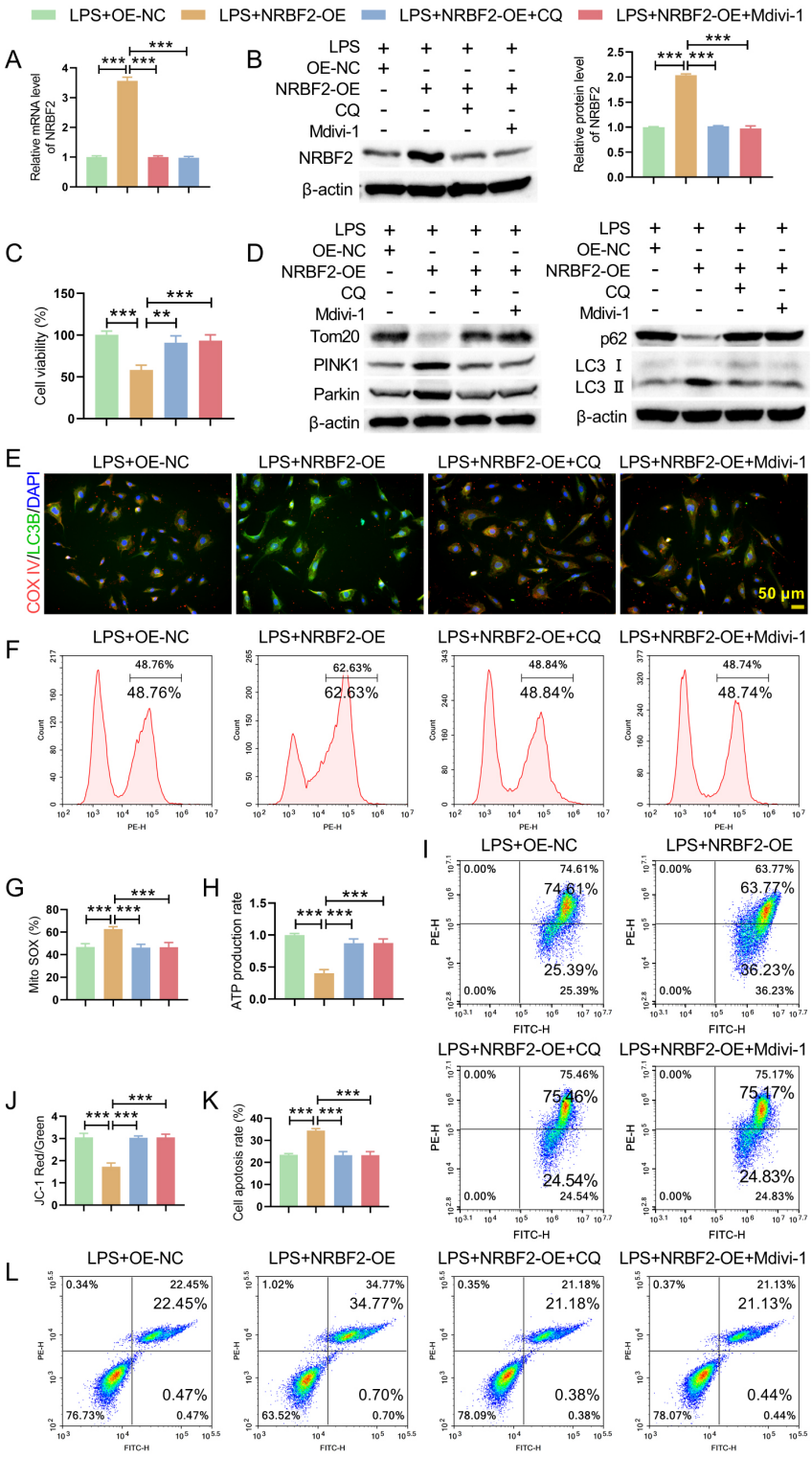


**Fig. 4. The effect of autophagy and mitophagy inhibitors on excessive mitophagy and mitochondrial dysfunction induced by NRBF2 overexpression.** Experimental groups: LPS+OE-NC, LPS+NRBF2-OE, LPS+NRBF2-OE+CQ, and LPS+NRBF2-OE+Mdivi-1. (A,B) The mRNA and protein expression levels of NRBF2 were assessed using qRT-PCR and WB. (C) CCK-8 was utilized to assess cell viability. (D) WB was performed to determine the expression levels of Tom20, PINK1, parkin, p62, and LC3-II/LC3-I. (E) The colocalization of LC3B with mitochondria was evaluated using IF. (F,G) Flow cytometry was employed to detect mtROS. (H) ATP production rate was confirmed using an enhanced ATP assay kit. (I,J) JC-1 staining was performed and analyzed using flow cytometry to examine mitochondrial membrane potential. (K,L) The apoptosis rate was measured using flow cytometry. n = 3. ** $p < 0.01$, *** $p < 0.001$ vs. LPS+OE-NC or LPS+NRBF2-OE. OE-NC, overexpression negative control; CQ, chloroquine.

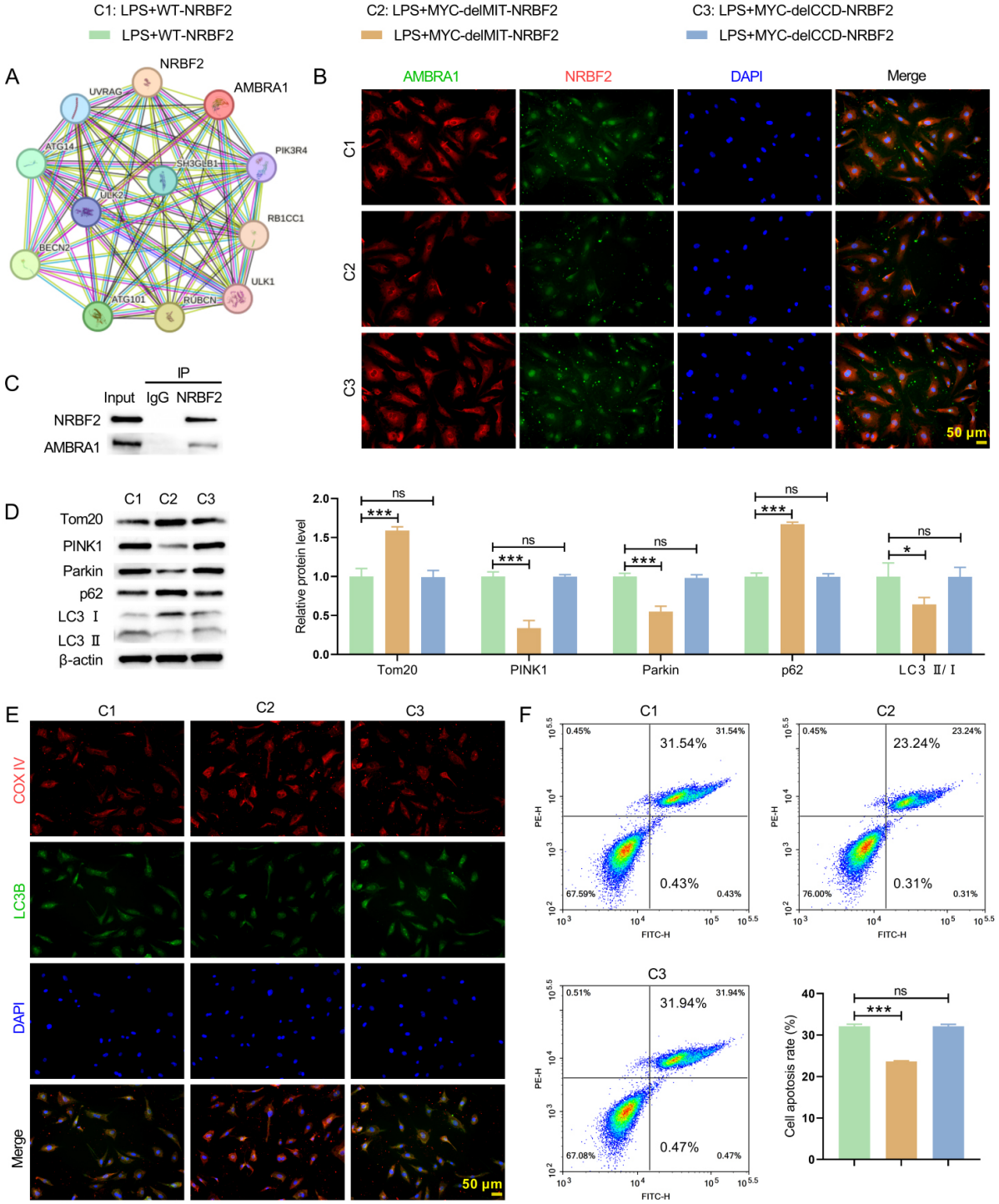


**Fig. 5. The effect of NRBF2–AMBRA1 interaction on mitophagy.** The constructed NRBF2 MIT-deficient plasmids were transfected into HPMECs. Experimental groups: LPS+WT-NRBF2, LPS+MYC–delMIT-NRBF2, and LPS+MYC-delCCD-NRBF2. (A) Predicting the interaction between NRBF2 and AMBRA1 using the STRING database. (B) IF was used to assess colocalization between NRBF2 and AMBRA1. (C) Co-IP was performed to examine the protein interaction between NRBF2 and AMBRA1. (D) The expression levels of Tom20, PINK1, parkin, p62, and LC3-II/LC3-I were evaluated using WB. (E) The colocalization between LC3B and mitochondria was observed using IF. (F) Flow cytometry was conducted to measure the apoptosis rate. n = 3. * $p < 0.05$, *** $p < 0.001$, ns means no significant difference vs. LPS+WT-NRBF2. AMBRA1, Autophagy and Beclin 1 Regulator 1; MIT, microtubule-interacting and trafficking; WT-NRBF2, Wild-type nuclear receptor binding factor 2; MYC–delMIT-NRBF2, MYC-tagged deletion of MIT domain of nuclear receptor binding factor 2; MYC-delCCD-NRBF2, MYC-tagged deletion of Coiled-Coil Domain of nuclear receptor binding factor 2; STRING, Search Tool for the Retrieval of Interacting Genes/Proteins; Co-IP, Co-immunoprecipitation.

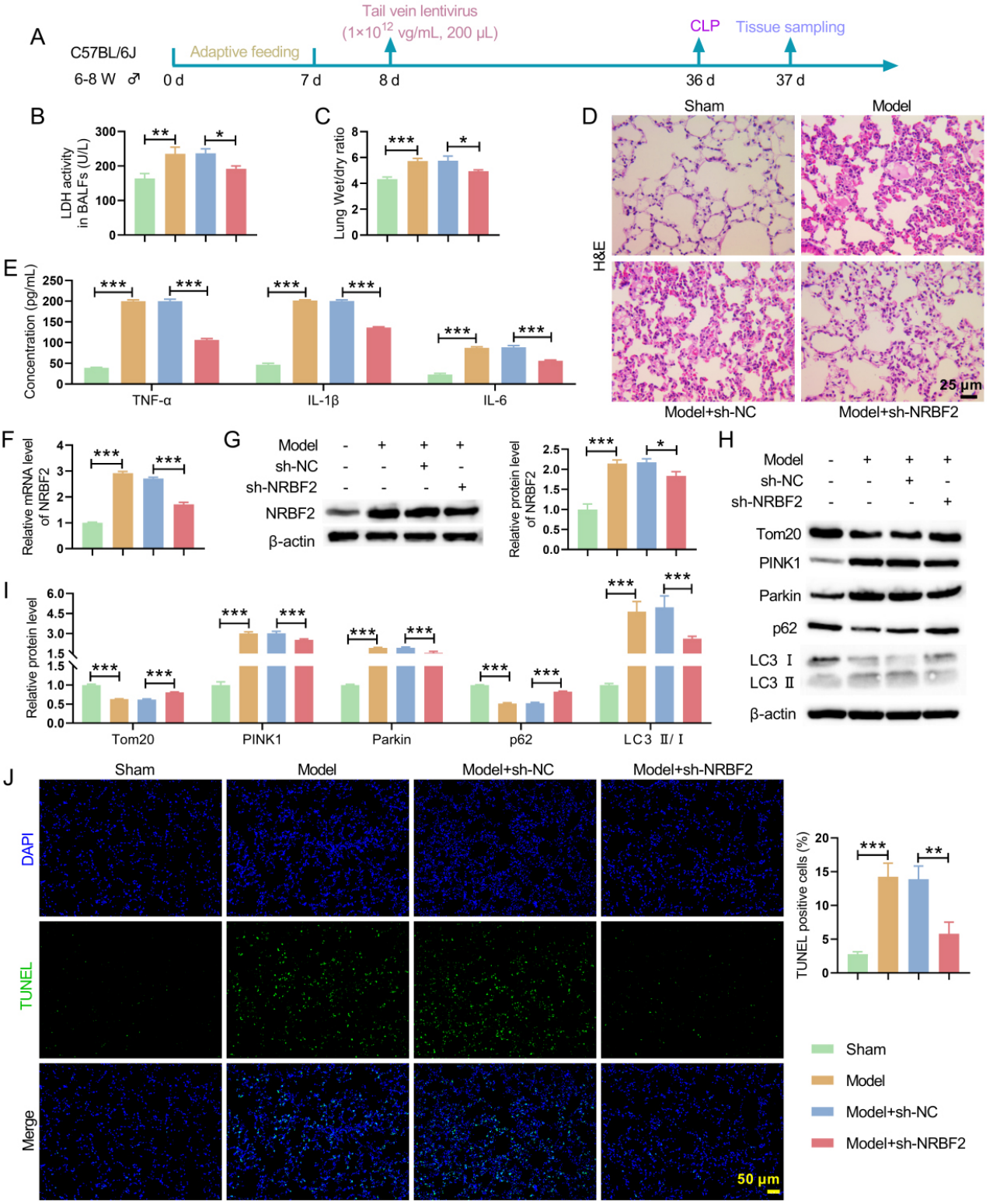


**Fig. 6. The effect of interfering with NRBF2 expression on ALI in sepsis.** Experimental groups: Sham, Model, Model+sh-NC, and Model+sh-NRBF2. (A) Animal experiment timeline. (B) The LDH assay kit was utilized to detect LDH activity in BALF. (C) Measurement of the lung wet weight/dry weight ratio. (D) H&E staining was performed to assess the pathological changes in the mouse lung tissue. (E) Serum levels of TNF-$\alpha$, IL-1$\beta$, and IL-6 were measured using ELISA. (F,G) The expression level of NRBF2 was evaluated using qRT-PCR and WB. (H,I) WB was used to assess the expression levels of Tom20, PINK1, parkin, p62, and LC3-II/LC3-I. (J) TUNEL staining was performed to detect the apoptosis rate in the lung tissue. n = 6 (B); n = 3 (C–J). * $p < 0.05$, ** $p < 0.01$, *** $p < 0.001$ vs. Sham or Model+sh-NC. TUNEL, Terminal deoxynucleotidyl transferase dUTP nick end labeling.

and neurological diseases [17,18]. This study reports for the first time that NRBF2 is significantly upregulated in both *in vivo* and *in vitro* models of sepsis-induced ALI. This upregulation, consistent with GEO database analysis, suggests a potential pathogenic role for NRBF2 in this condition. Kim *et al*. [10] identified that NRBF2-mediated excessive autophagy can induce malignant proliferation and radiation resistance in glioblastoma. However, another study has reported that the activation of NRBF2 can reduce neuroinflammation and oxidative stress induced by subarachnoid hemorrhage, thereby preventing early brain injury following subarachnoid hemorrhage [19]. This discrepancy indicates that NRBF2 may play dual roles in different disease contexts. Our study found that NRBF2 knockdown significantly improved the pathological features of sepsis-associated ALI. Therefore, NRBF2 may be a key regulatory molecule in sepsis-associated ALI, and its function may be highly correlated with autophagy.

Mitophagy is a key mechanism regulating sepsis-associated ALI as it protects against tissue damage by removing damaged mitochondria [20]. However, excessive activation of this process can exacerbate tissue injury [21]. The PINK1/parkin pathway is a classic mitophagy pathway [22]. A study has shown that under stimulatory conditions, PINK1 accumulates on the outer mitochondrial membrane and recruits parkin, which then ubiquitilates substrate proteins such as p62, thereby promoting the formation of autophagosomes. Finally, autophagosomes engulf damaged mitochondria via LC3 interaction, thereby completing mitophagy [23]. A previous study has documented that LPS can activate the PINK1/parkin pathway in ALI, leading to excessive mitophagy and lung injury [24]. Consistent with this observation, our study demonstrated that interfering with NRBF2 expression can inhibit the activation of the PINK1/parkin pathway, alleviate LPS-induced excessive mitophagy activation, and improve mitochondrial function. In addition, a bidirectional crosstalk exists between mitophagy, oxidative stress, and inflammatory responses. Oxidative stress and inflammation can impair autophagic flux, resulting in the accumulation of damaged proteins and organelles, including mitochondria. Damaged mitochondria, in turn, release large amounts of ROS, thereby exacerbating oxidative stress, activating toll-like receptors, and intensifying inflammatory responses, forming a vicious cycle that worsens sepsis-induced ALI [25,26]. The results of this study indicate that interfering with NRBF2 expression can suppress the release of inflammatory factors and mtROS. Nevertheless, the precise interrelationship among mitophagy, inflammation, and oxidative stress warrants further investigation.

In terms of molecular mechanisms, this study has, for the first time, revealed the specific mechanism by which NRBF2 interacts with AMBRA1 to regulate mitophagy. NRBF2 contains two distinct domains: an N-terminal MIT domain and a CCD domain [27]. The MIT domain of NRBF2 has been shown to play a crucial role in autophagy, whereas the CCD domain is nonessential [28]. The experiments in this study confirmed that deletion of the MIT domain disrupts NRBF2 binding to AMBRA1, thereby inhibiting downstream mitophagy. This finding not only clarifies the specific molecular mechanism by which NRBF2 regulates mitophagy but also suggests that AMBRA1, an autophagy-regulating protein, acts as a downstream target of NRBF2, influencing the activation and regulation of the autophagy signaling pathway and thereby playing a crucial role in sepsis-associated ALI. Similarly, in Wen *et al*.'s study [29], the AMBRA1–lysosome signaling pathway was observed to play a key role in small cell lung cancer. Therefore, developing specific inhibitors targeting the NRBF2–AMBRA1 interaction may provide a theoretical basis for new therapeutic strategies for sepsis-associated ALI.

This study revealed the key role of NRBF2 in regulating mitophagy in sepsis-induced ALI; however, certain limitations exist. First, CQ, a lysosomotropic agent that broadly inhibits autophagy at late stages, was primarily used. Although complementary data with Mdivi-1 support our conclusions, future studies employing more specific genetic interventions (e.g., knockdown of core mitophagy genes) would strengthen the causal link between NRBF2 and mitophagy in this model. Second, the specific regulatory mechanisms underlying NRBF2 upregulation in sepsis remain unclear, and future studies should employ transcriptomics and other technologies to investigate further. Third, this study used pulmonary microvascular endothelial cells, but sepsis-induced ALI involves multiple cell types, including alveolar epithelial cells and macrophages. Future studies should establish coculture systems that more closely mimic the *in vivo* microenvironment. Finally, sepsis often leads to multiorgan dysfunction, and it remains to be investigated whether NRBF2 plays a similar role in damage to other organs.

## Conclusion

In summary, this study confirms that NRBF2 is significantly upregulated in sepsis-induced ALI and interacts with AMBRA1 via its MIT domain to jointly regulate mitophagy. Interfering with NRBF2 expression can inhibit excessive mitophagy activation, improve mitochondrial function, and reduce lung tissue damage and inflammatory responses, thereby alleviating the pathological progression of sepsis-induced ALI. Therefore, this study suggests that NRBF2 is a potential therapeutic target for sepsis-induced ALI, providing direction for future research and treatment.

## Abbreviations

ALI, acute lung injury; AMBRA1, Autophagy and Beclin 1 Regulator 1; BALF, bronchoalveolar lavage fluid; BCA, bicinchoninic acid; CCK-8, Cell counting kit-8; CLP, cecal ligation and puncture; $CO_2$, carbon diox-

ide; Co-IP, Co-immunoprecipitation; CQ, chloroquine; DAPI, 4′,6-diamidino-2-phenylindole; ELISA, Enzyme-linked immunosorbent assay; FITC, fluorescein isothiocyanate; GEO, Gene Expression Omnibus; H&E, Hematoxylin and eosin; HPMECs, human pulmonary microvascular endothelial cells; IF, Immunofluorescence; IL-1$\beta$, Interleukin-1 beta; LDH, Lactate dehydrogenase; LPS, lipopolysaccharide; MIT, microtubule-interacting and trafficking; mtROS, Mitochondrial reactive oxygen species; NRBF2, Nuclear receptor binding factor 2; OD, optical density; PBS, phosphate-buffered saline; PINK1, PTEN-induced kinase 1; qRT-PCR, Quantitative real-time polymerase chain reaction; RIPA, radioimmunoprecipitation assay; shRNA, short hairpin RNA; TNF-$\alpha$, tumor necrosis factor-alpha; TUNEL, Terminal deoxynucleotidyl transferase dUTP nick end labeling; WB, Western blotting.

## Availability of Data and Materials

All data generated and/or analyzed during the current study are available from the corresponding author on reasonable request.

## Author Contributions

SL: Conceptualization, Investigation, Data curation, Formal analysis, Writing-original draft. WZ: Conceptualization, Investigation, Data curation, Formal analysis, Writing-original draft. YW: Formal analysis, Methodology. CL: Data curation, Software, Methodology. JZ: Conceptualization, Investigation, Project administration, Resources, Supervision, Funding, Writing-original draft. All authors contributed to the important editorial changes in the manuscript. All authors read and approved the final manuscript. All authors have participated sufficiently in the work to take public responsibility for appropriate portions of the content and agreed to be accountable for all aspects of the work in ensuring that questions related to its accuracy or integrity.

## Ethics Approval and Consent to Participate

All experimental protocols have been reviewed and approved by the Animal Ethics Committee of Guizhou Medical University (2503016). All procedures complied with the ARRIVE Guidelines 2.0.

## Acknowledgment

Not applicable.

## Funding

This study was supported by the Beijing iGandan Foundation (iGandanF-1082025-LG032).

## Conflict of Interest

The authors declare no conflict of interest.

## Supplementary Material

Supplementary material associated with this article can be found, in the online version, at https://doi.org/10.24976/Discov.Med.202638211.196.

## References

[1] Xu YF, Yang N, Hao PH, Wen R, Zhang TN. Molecular mechanisms and functions of protein acetylation in sepsis and sepsis-associated organ dysfunction. Cellular & Molecular Biology Letters. 2025; 30: 91. https://doi.org/10.1186/s11658-025-00773-z.

[2] Zhou Q, Zeng X, Kang W, Pan X, Wang L, Xia Z. Ciprofol attenuates sepsis-induced cardiomyopathy via $\alpha$7 nicotinic acetylcholine receptor-dependent modulation of myocardial inflammation and NF-κB/STAT3 signaling. European Journal of Pharmacology. 2025; 1003: 177983. https://doi.org/10.1016/j.ejphar.2025.177983.

[3] Liu D, Huang SY, Sun JH, Zhang HC, Cai QL, Gao C, *et al*. Sepsis-induced immunosuppression: mechanisms, diagnosis and current treatment options. Military Medical Research. 2022; 9: 56. https://doi.org/10.1186/s40779-022-00422-y.

[4] Zhang S, Jiang M, Wu C, Wang H, He F. Modulation of the CEACAM1/TIM3 pathway by traditional Chinese medicine Xuebijing alleviates sepsis-induced acute lung injury through inhibition of NETs formation. Journal of Ethnopharmacology. 2025; 353: 120280. https://doi.org/10.1016/j.jep.2025.120280.

[5] Baisheng S, Mingxing L, Jiaqi Z, Hongjun K, Hui L, Feihu Z. Acute lung injury caused by sepsis: how does it happen? Front. Med. 2023; 10: 1289194. https://doi.org/10.3389/fmed.2023.1289194.

[6] Hu S, Hu J, Shu S, Chen Y, Wang L. Interfering with USP50 expression inhibits macrophage pyroptosis in sepsis-induced acute lung injury by degrading NLRP3 protein. Scientific Reports. 2025; 15: 26768. https://doi.org/10.1038/s41598-025-11224-2.

[7] Han H, Zhang Y, Huang E, Zhou S, Huang Z, Qin K, *et al*. The role of TBC1D15 in sepsis-induced acute lung injury: Regulation of mitochondrial homeostasis and mitophagy. International Journal of Biological Macromolecules. 2025; 293: 139289. https://doi.org/10.1016/j.ijbiomac.2024.139289.

[8] Xiao Z, Long J, Zhang J, Qiu Z, Zhang C, Liu H, *et al*. Administration of protopine prevents mitophagy and acute lung injury in sepsis. Frontiers in Pharmacology. 2023; 14: 1104185. https://doi.org/10.3389/fphar.2023.1104185.

[9] Ling J, Yu S, Xiong F, Xu T, Li S. Melatonin Attenuates Sepsis-Induced Acute Lung Injury via Inhibiting Excessive Mitophagy. Drug Design, Development and Therapy. 2023; 17: 2775–2786. https://doi.org/10.2147/DDDT.S423264.

[10] Kim J, Kang H, Son B, Kim MJ, Kang J, Park KH, *et al*. NRBF2-mediated autophagy contributes to metabolite replenishment and radioresistance in glioblastoma. Experimental & Molecular Medicine. 2022; 54: 1872–1885. https://doi.org/10.1038/s12276-022-00873-2.

[11] Shen W, Luo P, Sun Y, Zhang W, Zhou N, Zhan H, *et al*. NRBF2 regulates the chemoresistance of small cell lung cancer by interacting with the P62 protein in the autophagy process. iScience. 2022; 25: 104471. https://doi.org/10.1016/j.isci.2022.104471.

[12] Wu S, Zhuang H, Zhou X, Li K. NRBF2 plays a crucial role in the acquisition process of learning and memory, inde-

pendent of the Vps34 complex. Frontiers in Behavioral Neuroscience. 2025; 19: 1529522. https://doi.org/10.3389/fnbeh.2025.1529522.

[13] Qu X, Li XY, Feng Y, Wang X, Li L, Wang YP, *et al*. sh- Ambra1 inhibits IRS-1/PI3K/Akt signalling pathway to reduce autophagy in gestational diabetes. Endokrynologia Polska. 2024; 75: 61–70. https://doi.org/10.5603/ep.95519.

[14] Di Rienzo M, Romagnoli A, Ciccosanti F, Refolo G, Consalvi V, Arena G, *et al*. AMBRA1 regulates mitophagy by interacting with ATAD3A and promoting PINK1 stability. Autophagy. 2022; 18: 1752–1762. https://doi.org/10.1080/15548627.2021.1997052.

[15] Wang J, Fu H, Wang B, Yu J, Liu X, Liu Y, *et al*. Carbazochrome attenuates acute lung injury in septic rats by inhibition of Parkin-mediated mitochondrial autophagy. Journal of Radiation Research and Applied Sciences. 2022; 15: 12–20. https://doi.org/10.1016/j.jrras.2022.05.017.

[16] Zou S, Bai J, Liang C, Yang J, Xiao J. Plasmacytoid dendritic cells in sepsis-associated acute lung injury: a potential therapeutic target. Anesthesiology and Perioperative Science. 2025; 3: 36. https://doi.org/10.1007/s44254-025-00121-6.

[17] Tian Y, Xie B, Wang S, Ma X, Deng H, Ma L, *et al*. PRKD3 promotes proliferation of liver cancer cells: a downstream proteomics profiling study. American Journal of Translational Research. 2024; 16: 6384–6398. https://doi.org/10.62347/YLJE5332.

[18] Zhang SQ, Deng Q, Zhu Q, Hu ZL, Long LH, Wu PF, *et al*. Cell type-specific NRBF2 orchestrates autophagic flux and adult hippocampal neurogenesis in chronic stress-induced depression. Cell Discovery. 2023; 9: 90. https://doi.org/10.1038/s41421-023-00583-7.

[19] Zeng H, Chen H, Li M, Zhuang J, Peng Y, Zhou H, *et al*. Autophagy protein NRBF2 attenuates endoplasmic reticulum stress-associated neuroinflammation and oxidative stress via promoting autophagosome maturation by interacting with Rab7 after SAH. Journal of Neuroinflammation. 2021; 18: 210. https://doi.org/10.1186/s12974-021-02270-4.

[20] Zhang Z, Chen Z, Liu R, Liang Q, Peng Z, Yin S, *et al*. Bcl-2 Proteins Regulate Mitophagy in Lipopolysaccharide-Induced Acute Lung Injury via PINK1/Parkin Signaling Pathway. Oxidative Medicine and Cellular Longevity. 2020; 2020: 6579696. https://doi.org/10.1155/2020/6579696.

[21] Shi J, Piao M, Liu C, Yang J, Guan X, Liu H, *et al*. Electroacupuncture pretreatment maintains mitochondrial quality control via HO-1/MIC60 signaling pathway to alleviate endotoxin-induced acute lung injury. Biochimica et Biophysica Acta. Molecular Basis of Disease. 2024; 1870: 167480. https://doi.org/10.1016/j.bbadis.2024.167480.

[22] Wang J, Sun Z, Jiang L, Xuan L, Ma Y, Wang J, *et al*. Activation of Pink1/Parkin-mediated mitochondrial autophagy alleviates exertional heat stroke-induced acute lung injury in rats. Clinical Hemorheology and Microcirculation. 2024; 88: 13–31. https://doi.org/10.3233/CH-242100.

[23] Wang J, Meng R, Sun Z, Xuan L, Wang J, Gu Y, *et al*. Protection of Parkin over-expression on lung in rats with exertional heat stroke by activating mitophagy. BMC Pulmonary Medicine. 2024; 24: 431. https://doi.org/10.1186/s12890-024-03222-3.

[24] Zhao R, Wang B, Wang D, Wu B, Ji P, Tan D. Oxyberberine Prevented Lipopolysaccharide-Induced Acute Lung Injury through Inhibition of Mitophagy. Oxidative Medicine and Cellular Longevity. 2021; 2021: 6675264. https://doi.org/10.1155/2021/6675264.

[25] Ryter SW, Choi AMK. Autophagy in lung disease pathogenesis and therapeutics. Redox Biology. 2015; 4: 215–225. https://doi.org/10.1016/j.redox.2014.12.010.

[26] Mohsin M, Zaki A, Tabassum G, Khan S, Ali S, Ahmad T, *et al*. Urolithin-A supplementation alleviates sepsis-induced acute lung injury by reducing mitochondrial dysfunction and modulating macrophage polarization. Mitochondrion. 2025; 84: 102047. https://doi.org/10.1016/j.mito.2025.102047.

[27] Wu MY, Cai CZ, Yang C, Yue Z, Chen Y, Bian ZX, *et al*. Emerging roles of NRBF2/PI3KC3 axis in maintaining homeostasis of brain and guts. Neural Regeneration Research. 2022; 17: 323–324. https://doi.org/10.4103/1673-5374.317973.

[28] Ohashi Y, Soler N, García Ortegón M, Zhang L, Kirsten ML, Perisic O, *et al*. Characterization of Atg38 and NRBF2, a fifth subunit of the autophagic Vps34/PIK3C3 complex. Autophagy. 2016; 12: 2129–2144. https://doi.org/10.1080/15548627.2016.1226736.

[29] Wen Y, Sun X, Zeng L, Liang S, Li D, Chen X, *et al*. CDK4/6 Inhibitors Impede Chemoresistance and Inhibit Tumor Growth of Small Cell Lung Cancer. Advanced Science (Weinheim, Baden-Wurttemberg, Germany). 2024; 11: e2400666. https://doi.org/10.1002/advs.202400666.